Research Square

Preprints are preliminary reports that have not undergone peer review.
They should not be considered conclusive, used to inform clinical practice,
or referenced by the media as validated information.

Diet and digestive traits associated with crab digestion in the crab-eating frog (Fejervarya cancrivora)

Tian Lan
Hainan Normal University College of Life Sciences
Mianjun Chen
Hainan Normal University College of Life Sciences
Meiling Hong
Hainan Normal University College of Life Sciences
Lijun Wang
wanglijun_haikou@hainnu.edu.cn

Hainan Normal University College of Life Sciences https://orcid.org/0009-0004-7592-2517

Research Article

Keywords: Crab-eating frog, stomach flushing, digestive enzyme activity, gut microbiota, chitin digestion, metagenomics

Posted Date: September 29th, 2026

DOI: https://doi.org/10.21203/rs.3.rs-11061922/v1

License: This work is licensed under a Creative Commons Attribution 4.0 International License.
Read Full License

Diet and digestive traits associated with crab digestion in the crab-eating frog (*Fejervarya cancrivora*)

Tian Lan[1], Mianjun Chen[1], Meiling Hong[1], Lijun Wang*[1]

[1]Ministry of Education Key Laboratory for Ecology of Tropical Islands, Key Laboratory of Tropical Animal and Plant Ecology of Hainan Province, College of Life Sciences, Hainan Normal University, Haikou 571158, Hainan, China

Email addresses

Tian Lan: lant54354@gmail.com

Mianjun Chen: 1577968764@qq.com

Meiling Hong: mlhong@hainnu.edu.cn

Lijun Wang: wanglijun_haikou@hainnu.edu.cn

*Corresponding author. E-mail: wanglijun_haikou@hainnu.edu.cn

Abstract: Despite their mechanically resistant, chitin-rich exoskeletons, how anurans with limited chewing capacity utilize crustacean prey remains poorly understood. The crab-eating frog (*Fejervarya cancrivora*), which inhabits mangrove and brackish-water environments and feeds on crustaceans, provides a suitable model system for addressing this question. However, how its natural diet relates to host digestive traits and gut microbial functional potential remains unclear. To address this, we combined stomach-content analysis via stomach flushing with gastrointestinal histology, digestive enzyme assays, and gut metagenomics to examine crustacean consumption in relation to host digestive characteristics and microbial functional potential. The results showed that decapods dominated stomach contents by volume, accounting for 83.50% in males

and 92.83% in females. The stomach exhibited prominent longitudinal folds and circular, oblique and longitudinal muscle bundles, consistent with food accommodation, mixing and propulsion. Chitinase activity was detected in the stomach, small intestine and large intestine, indicating chitin-hydrolysing capacity at multiple gastrointestinal sites. Gut metagenomes harboured genes spanning chitin polymer cleavage, chitooligosaccharide and chitobiose processing, N-acetylglucosamine (GlcNAc) transport, and intracellular metabolism, with distinct candidate source genera at each stage: *Plesiomonas* and *Aeromonas* (polymer cleavage), *Candidatus* Avirikenella and *Ruthenibacterium* (chitooligosaccharide and chitobiose processing), *Cetobacterium* (GlcNAc transport), and *Mucinivorans*, *Parabacteroides*, and *Alistipes* (intracellular metabolism). These annotations indicate that genes associated with different stages of chitin utilization are distributed across multiple bacterial genera. Together, these findings link crustacean consumption in *F. cancrivora* to gastrointestinal structural traits, chitin-hydrolysing capacity, and gut microbial functional potential, offering an ecophysiological perspective on how anurans process and utilize chitin-rich animal prey.

Keywords: Crab-eating frog; stomach flushing; digestive enzyme activity; gut microbiota; chitin digestion; metagenomics

Background

The ability of animals to exploit food resources depends not only on food acquisition but also on constraints imposed by food structure and digestive capacity [1]. In crustaceans of chitin-rich exoskeletons, chitin forms a composite with proteins and minerals, which provides high mechanical strength but may restrict enzyme access to

substrates [2, 3]. Thus, for vertebrates feeding on crustaceans, breaking down the mechanically resistant exoskeleton and subsequently hydrolysing and utilizing its chitin represent major digestive challenges inherent to the use of these food resources [2-5].

Studies in mice and myrmecophagous mammals, including the giant anteater (*Myrmecophaga tridactyla*), aardvark (*Orycteropus afer*) and Temminck's pangolin (*Smutsia temminckii*), indicate that the processing of chitin-rich foods may involve both host digestive mechanisms and gut microbial functions [4-6]. In anurans, gastrointestinal motility facilitates food mixing and propulsion, and chitinolytic enzymes have been reported in the stomach and pancreas of some frogs [7-9]. Gut microbial communities in myrmecophagous mammals also harbour genes associated with chitin degradation and the metabolism of its breakdown products [6, 10]. However, previous studies have generally examined host digestive structure, digestive enzymes, and the gut microbiota separately, and relatively few have taken natural diet composition as a starting point to test whether digestive traits across these levels correspond to the food resources actually used by animals [6, 11, 12]. This relationship is particularly worth examining in wild vertebrates that naturally and persistently exploit chitin-rich animal prey [10-13].

The crab-eating frog (*Fejervarya cancrivora*) inhabits mangrove and brackish-water environments, where field studies have documented its consumption of crabs and other crustaceans [14-16]. Most adult anurans swallow prey with limited oral processing, whereas crustaceans such as crabs possess mechanically resistant exoskeletons [2, 17]. This mismatch between feeding mode and food structure makes

F. cancrivora a valuable natural system for examining how vertebrates process and utilize chitin-rich animal prey [2, 14, 16, 17]. Although recent work has characterized host chitinolytic capacity and gut microbial functional potential in this species, direct evidence linking these digestive traits to its natural crustacean-rich diet in the wild remains limited [18].

Here, we examined the contribution of crustaceans to the natural diet of *F. cancrivora* and whether this dietary pattern was reflected in digestive traits at both host and microbial levels. Stomach contents obtained by stomach flushing were analysed to characterize diet composition. Gastrointestinal histology was then combined with digestive enzyme assays to assess the structural and enzymatic basis of host digestion. Metagenomic analysis of intestinal contents characterized gut microbial composition and the functional potential for chitin degradation and the metabolism of its breakdown products. Together, these analyses integrate natural diet composition, host digestive traits, and microbial functional potential within a common ecophysiological framework.

Methods

Study Area and Sample Collection

A total of 124 adult *F. cancrivora* (42 males and 82 females) were collected from the mangrove areas in the Hainan Dongzhaigang National Nature Reserve (110°32′–110°37′ E, 19°51′–20°01′ N, Haikou, China) between April and September 2023. Stomach contents were obtained by stomach flushing for dietary analysis. Fifteen adults were transported to the laboratory for further analyses, while the remaining individuals were released at their capture sites.

The 15 frogs retained for laboratory analyses were euthanized by double pithing and dissected, and the lengths of individual digestive tract segments were recorded. For histology, tissue samples from the tongue, esophagus, stomach, small intestine, large intestine, liver, and pancreas were fixed in Bouin's solution (n=3). Tissues from the stomach, small intestine, and large intestine were collected for digestive enzyme activity assays (n=6), while intestinal contents from six individuals were collected for metagenomic analysis. All procedures involving animals were approved by the Animal Ethics Committee of the Hainan Ecological and Environmental Education Center (approval no. HNECEE-2020-003).

Identification of Stomach Contents and Dietary Analysis

Stomach contents were preserved in 70% ethanol and examined under an EZ4 W stereomicroscope (Leica, Wetzlar, Germany). Prey items were identified to the lowest possible taxonomic level based on diagnostic morphological features and classified as terrestrial or aquatic according to their typical habitats [19]. Materials considered to have been ingested incidentally during prey capture, such as mangrove leaves, were excluded from quantitative analyses. For each intact prey item, length (L) and maximum width (W) were measured, and volume was estimated using the prolate spheroid formula: $V = 4\pi(L/2)(W/2)^2/3$ [20]. For male and female frogs separately, we calculated the numerical percentage (N%), relative frequency of occurrence (F%), and volumetric percentage (V%) of each prey taxon. These indices were calculated as follows:

$$N_i\% = N_i/\sum n_i \times 100 \quad (1)$$

$$F_i\% = f_i / \sum f_i \times 100 \quad (2)$$

$$V_i\% = v_i / \sum v_i \times 100 \quad (3)$$

Where n_i is the number of prey items in category i, f_i is the number of occurrences of prey category i, and v_i is the total volume of prey category i. The index of relative importance (IRI) was calculated as follows [20]:

$$IRI_i = F_i\% \times (N_i\% + V_i\%) \quad (4)$$

The N%, F%, V%, and IRI values were summarized separately at the order and family levels. Family-level IRI values were calculated from the corresponding family-level N%, F%, and V% values. At the order level, N%, F%, and V% were obtained by summing the corresponding values of the constituent families, and order-level IRI was calculated as the sum of the IRI values of those families. Dietary diversity and niche breadth were calculated using the numerical proportions of prey at the family level. The Shannon–Wiener diversity index was calculated as follows [21]:

$$H' = -\sum P_i log_2 P_i \quad (5)$$

The evenness index was calculated as follows:

$$E = H' / log_2 S \quad (6)$$

Levins' niche breadth was calculated as follows:

$$B = 1 / \sum P_i^2 \quad (7)$$

where P_i is the proportion of prey items belonging to family i among all prey items recorded for the corresponding sex, and S is the number of prey families detected for that sex. The total number of prey items recovered from each non-empty stomach was recorded as the number of prey items per stomach. Empty stomachs were included only

when calculating the proportion of empty stomachs and were excluded from the mean number of prey items per stomach and all dietary index calculations.

Histological Examination of the Digestive System

After fixation in Bouin's solution for 24 h, tissue samples were transferred to 70% ethanol and processed for paraffin embedding. Serial sections (4–5 μm thick) were cut using an RM2016 microtome (Leica, Wetzlar, Germany) and stained with hematoxylin and eosin (H&E). Sections were examined and imaged using an Eclipse E100 light microscope with a DS-U3 camera control unit (Nikon, Tokyo, Japan). For each animal, three sections were examined from each digestive tract region, and six standardized microscopic fields were selected from each section. Mucosal surface architecture, epithelial type, glandular composition, and muscle-layer organization were recorded for each region of the digestive tract. An ocular micrometer was used to measure digestive-tract wall and mucosal thicknesses, villus dimensions, and muscle-layer thickness. Histomorphometric measurements were summarized using descriptive statistics, with no inferential comparisons performed among digestive-tract regions.

Digestive Enzyme Activity Assays

After their contents were removed, stomach, small-intestinal, and large-intestinal tissues were rinsed with phosphate-buffered saline (PBS; Wuhan Servicebio Technology Co., Ltd., Wuhan, China) and blotted dry. Approximately 0.1 g of each tissue was combined with 1 mL of extraction buffer and homogenized on ice. The homogenates were centrifuged at 10,000 rpm for 10 min at 4°C, and the supernatants were collected as crude enzyme extracts. All enzyme assays were completed within 8

h. Soluble protein concentrations were determined using a bicinchoninic acid (BCA) assay, and the activities of pepsin (ZIKER163), trypsin (ZIKER524), lipase (ZIKER529), and chitinase (ZIKER592) were measured using the corresponding commercial assay kits, all obtained from Shenzhen Ziker Biological Technology Co., Ltd. (Shenzhen, China), according to the manufacturer's instructions. Enzyme activities were normalized to soluble protein content and expressed as U mg^{-1} protein.

Gut Metagenomic Sequencing and Functional Annotation

The six intestinal-content samples described above (LI_R1–LI_R6) were submitted to Shanghai Majorbio Bio-pharm Technology Co., Ltd. (Shanghai, China) for metagenomic sequencing. DNA concentration was measured using a Quantus Fluorometer with PicoGreen, and DNA integrity was assessed by 1% agarose gel electrophoresis. All six samples met the quality requirements for library construction. DNA was fragmented to approximately 350 bp using a Covaris M220 instrument, followed by paired-end library construction and sequencing on an Illumina NovaSeq X Plus platform.

Raw metagenomic reads were quality-filtered using fastp v0.23.0 [22], and host-derived sequences were removed using Bowtie2 v2.5.4 [23] against the host reference genome from Ensembl Release 104. The remaining non-host reads were assembled using MEGAHIT v1.2.9 [24], and open reading frames were predicted using Prodigal v2.6.3 [25]. Predicted genes ≥ 100 bp were retained for downstream analysis. A non-redundant gene catalog was constructed using CD-HIT v4.6.1 [26], with the longest sequence in each cluster retained as the representative sequence. Gene abundances were

quantified using Salmon v1.10.3 [27]. Taxonomic and functional annotations of the non-redundant genes were performed against the NCBI non-redundant protein (NR), Kyoto Encyclopedia of Genes and Genomes (KEGG) [28], and Carbohydrate-Active enZymes (CAZy) [29] databases. NR and KEGG annotations were assigned using DIAMOND v2.0.13 [30], whereas CAZy annotations were assigned using HMMER v3.1b2 [31] with an E-value cutoff of 1×10^{-5}.

Genus-level taxonomic composition of the gut microbiota was characterized from the NR annotations, and the relative abundance of each genus was calculated from transcripts per million (TPM) values. Genera previously reported to be associated with chitin degradation or utilization were selected based on published studies.

Overall functional composition was assessed using the KEGG annotations, and the major functional categories were summarized at KEGG Level 2. Candidate glycoside hydrolase (GH) families associated with the degradation or utilization of chitin, chitooligosaccharides, N-acetylglucosamine (GlcNAc), and chitosan were then identified from the CAZy annotations according to CAZy family descriptions. Candidate GH families were classified according to their putative roles in chitin polymer cleavage, chitooligosaccharide processing, and chitobiose utilization. KEGG-annotated genes involved in product transport and intracellular metabolism were subsequently integrated with these GH families to reconstruct a putative chitin degradation and utilization pathway. Finally, key functional genes were linked to NR taxonomic annotations to identify their likely genus-level sources, and the relative contribution of each genus within each functional stage was calculated from the

normalized abundances of the corresponding target genes. Genera not shown individually were grouped as Others.

Statistical Analysis

Dietary data were analyzed using SPSS version 10.0. The number of prey items per non-empty stomach was compared between males and females using a Mann–Whitney U test, whereas all other dietary indices were summarized using descriptive statistics. Digestive enzyme activity data were presented as the mean ± standard deviation (SD) and summarized descriptively. Figures were generated in R version 4.6.0, primarily using the ggplot2, patchwork, and vegan packages, and exported using ragg and svglite.

Results

Diet Composition

Stomach contents were obtained by stomach flushing from 120 of the 124 adults examined, comprising 41 males and 79 females, yielding a non-empty stomach rate of 96.8%. A total of 437 prey items, representing 6 classes, 15 orders, and 35 families, were identified (Additional file 1: Table S1). Non-empty stomachs contained an average of 3.6 ± 2.9 prey items. In total, 154 and 283 prey items were recovered from males and females, respectively. The mean number of prey items per non-empty stomach was 3.8 ± 2.9 for males and 3.6 ± 2.8 for females, with no statistically significant difference between the sexes ($Z = -0.438$, $P = 0.662$; Table 1).

Table 1. Summary of stomach-flushing samples and dietary diversity in *F. cancrivora*.

Metric	Overall	Male	Female
Sample size (individuals)	124	42	82
Non-empty stomachs, n (%)	120 (96.8%)	41 (97.6%)	79 (96.3%)
Number of prey items	437	154	283
Taxonomic richness	6 classes, 15 orders, 35 families	5 classes, 13 orders, 25 families	6 classes, 14 orders, 30 families
Prey items per non-empty stomach	3.6 ± 2.9	3.8 ± 2.9	3.6 ± 2.8
Shannon–Wiener diversity index (H′)	—	3.5661	3.5040
Evenness index (E)	—	0.7679	0.7141
Levins' niche breadth (B)	—	8.2164	6.7459

Note: Only non-empty stomachs were included when calculating the mean number of prey items per stomach; values are presented as the mean ± SD. An em dash (—) indicates that the overall index was not calculated.

At the order level, decapoda was the dominant prey group in the stomach contents of both sexes. In males, the percentage by number (N%), frequency (F%), and volume (V%) for decapoda were 51.95%, 47.66%, and 83.50%, respectively, with a summed family-level index of relative importance (IRI) of 2189.54. The corresponding values in females were 62.55%, 52.35%, and 92.83%, respectively, with an IRI of 2895.10 (Fig. 1a; Additional file 1: Table S2). Thus, compared with other prey orders, decapods accounted for a large proportion of prey items and contributed particularly strongly to

total stomach-content volume.

At the family-level, the principal prey families all belonged to Decapoda. The IRI values for Grapsidae were 1064.79 in males and 1999.35 in females, whereas those for Ocypodidae were 869.65 and 490.44, respectively. The corresponding values for Palaemonidae were 254.18 and 404.35. Together, these three families represented the most important prey groups for both sexes (Fig. 1b). In males and females, respectively, the Shannon–Wiener diversity indices were 3.5661 and 3.5040, and the evenness indices were 0.7679 and 0.7141. The corresponding Levins' niche breadth values were 8.2164 and 6.7459. These results indicated that although the stomach contents included multiple prey taxa, both numerical and volumetric contributions were strongly concentrated in Decapoda, particularly Grapsidae, Ocypodidae, and Palaemonidae.

Morphology and Histology of the Digestive System

The oropharyngeal cavity measured 25.10 ± 4.36 mm in length and contained 2–6 mucosal folds. The tongue exhibited filiform and fungiform papillae, lingual glands, and skeletal muscle bundles arranged in multiple directions (Fig. 2a, b). The esophagus was characterized by 9–13 longitudinal mucosal folds, abundant goblet cells and esophageal glands, and circular and longitudinal smooth muscle layers (Fig. 2c, d; Table 2).

The stomach exhibited 4–7 prominent longitudinal folds, and the cardiac, body and pyloric regions were clearly distinguished (Fig. 2e, f; Table 2). Wall thickness averaged 807.3 ± 148.9 μm in the cardia, 1088.1 ± 198.6 μm in the body, and 509.0 ± 94.3 μm in the pylorus, with the gastric body exhibiting the greatest thickness. The

gastric mucosa was lined by a simple columnar epithelium and formed gastric pits. Glandular composition varied among the stomach regions, with serous acini predominating in the cardiac and body glands and mucous acini in the pyloric glands. The muscular layer contained circular, oblique, and longitudinal bundles.

The small intestine measured 137.7 ± 35.1 mm and comprised the duodenum and ileum. Duodenal villi were branched and leaf-shaped, whereas the ileal mucosa formed oblique, overlapping folds with densely packed villi (Fig. 2g; Table 2). Both regions were lined by a simple columnar epithelium containing goblet cells. The large intestine had a wide lumen with semilunar folds formed by the mucosa and submucosa. These folds were lined by a simple columnar epithelium containing goblet cells. A distinct muscularis mucosae was not evident. The muscular layer comprised an inner circular and an outer longitudinal smooth muscle (Fig. 2h; Table 2).

The liver exhibited cords of hepatocyte surrounding central veins, with hepatic sinusoids and pigment cells scattered throughout the parenchyma (Fig. 3a). The pancreas showed a compound tubuloacinar organization with acinar cells, ducts and pancreatic islets (Fig. 3b).

Table 2. Histomorphometric measurements of major digestive tract regions in *F. cancrivora*.

Region	Parameter	Value
Oropharyngeal cavity	Length (mm)	25.10 ± 4.36
	Mucosal fold height (μm)	121.0 ± 11.4
Esophagus	Wall thickness (μm)	733.9 ± 18.2

	Mucosal thickness (μm)	651.5 ± 10.9
Gastric cardia	Wall thickness (μm)	807.3 ± 148.9
Gastric body	Wall thickness (μm)	1088.1 ± 198.6
Gastric pylorus	Wall thickness (μm)	509.0 ± 94.3
Small intestine	Length (mm)	137.7 ± 35.1
Duodenum	Villus length (μm)	359.3 ± 110.9
	Villus width (μm)	69.1 ± 19.8
	Muscular layer thickness (μm)	52.9 ± 5.3
Ileum	Villus length (μm)	630.9 ± 91.1
	Villus width (μm)	139.1 ± 21.9
	Muscular layer thickness (μm)	Approximately 51.5
Large intestine	Muscular layer thickness (μm)	60.5 ± 19.1

Note: Values are presented as mean ± SD, except for ileal muscular layer thickness, which was recorded as an approximately in the original measurements.

Digestive Enzyme Activities

Enzymes involved in the hydrolysis of chitin, proteins, and lipids were detected in different regions of the digestive tract (Table 3). Pepsin activity was detected only in the stomach and averaged 3.2 ± 0.5 U mg^{-1} pro. Trypsin activity was 45.0 ± 5.7 U mg^{-1} pro. in the small intestine and 44.8 ± 8.1 U mg^{-1} pro. in the large intestine. Chitinase activity was detected in the stomach, small intestine, and large intestine, with activities of 21.7 ± 2.0, 19.8 ± 2.0, and 20.1 ± 2.3 U mg^{-1} pro. Lipase activity averaged 101.4 ± 9.1 U mg^{-1} pro. in the small intestine and 111.4 ± 16.0 U mg^{-1} pro. in the large intestine.

Thus, chitinase activity was present in all three digestive tract regions examined.

Table 3. Digestive enzyme activities in different digestive tract regions of *F. cancrivora*

Digestive tract region	Pepsin	Trypsin	Chitinase	Lipase
Stomach	3.2 ± 0.5	—	21.7 ± 2.0	—
Small intestine	—	45.0 ± 5.7	19.8 ± 2.0	101.4 ± 9.1
Large intestine	—	44.8 ± 8.1	20.1 ± 2.3	111.4 ± 16.0

Note: Values are presented as mean ± SD. Enzyme activities are reported as U mg^{-1} protein. A dash (—) denotes the absence of a corresponding measurement in the original dataset.

Genus-Level Composition of the Gut Microbiota and Relative Abundance of Genera Reported to Degrade Chitin

Genus-level community composition varied among samples (Fig. 4a). Across the six samples, the most abundant genera were *Bacteroides* (7.626%), *Cetobacterium* (7.625%), *Alistipes* (7.533%), *Parabacteroides* (5.998%), and *Clostridium* (3.572%). The 20 taxa shown in Fig. 4a together accounted for 55.477% of the community, while the remaining taxa, grouped as Others, accounted for 44.523%.

Using a literature-derived list of 31 genera reported to include chitin-degrading members, we screened the NR-based taxonomic profiles of *F. cancrivora* gut metagenomes for these genera (Fig. 4b). Among them, *Bacteroides* [32] had the highest mean relative abundance (7.626%), followed by *Clostridium* [32], *Aeromonas* [33], and *Plesiomonas* [34], at 3.572%, 1.481%, and 1.250%, respectively. The mean relative

297 abundances of *Acinetobacter* [35], *Vibrio* [36], *Pseudomonas* [37], and *Photobacterium*
298 [38] were 0.773%, 0.608%, 0.439%, and 0.310%, respectively. The 18 genera with
299 mean relative abundances below 0.1% collectively accounted for 0.451% [39-46]
300 (Additional file 1: Table S3).

301 **Functional Potential of the Gut Microbiota to Utilize Chitin and Its Degradation**
302 **Products**

303 All samples contained genes assigned to the KEGG categories Carbohydrate
304 metabolism and Membrane transport, both of which include functions relevant to the
305 downstream utilization of chitin-derived products (Fig. 5).

306 Joint analysis of CAZy and KEGG annotations identified genes with predicted
307 roles spanning chitin polymer cleavage, chitooligosaccharide and chitobiose processing,
308 GlcNAc transport, and intracellular metabolism (Fig. 6; Additional file 1: Table S4).
309 Genes annotated as GH18 chitinase (K01183), GH18 endo-chitodextrinase (K21606),
310 and GH19/GH19_1 putative chitinase (K03791) represented the chitin polymer-
311 cleavage step and could generate shorter chitooligosaccharides and chitobiose.
312 Downstream, *nagZ* (K01207) was associated with further hydrolysis of
313 chitooligosaccharides and the release of GlcNAc. GH94–ChbP (K18675) represented
314 an alternative phosphorolytic route for chitobiose utilization, yielding GlcNAc and
315 GlcNAc-1-P. Potential GlcNAc uptake routes were encoded by *nagE*, a component of
316 the phosphotransferase system (PTS), and the *ngcE–ngcF–ngcG* ABC transporter
317 genes. The PTS could couple GlcNAc uptake to the formation of GlcNAc-6-P, whereas
318 GlcNAc entering through other transport routes could be phosphorylated to GlcNAc-6-

P by NagK. Annotations for NagA and NagB were consistent with the sequential conversion of GlcNAc-6-P to GlcN-6-P and then to Fru-6-P, thereby linking chitin-derived products to downstream carbohydrate metabolism.

Taxonomic assignment of the target functional genes revealed distinct profiles of candidate source genera across functional stages (Fig. 6). For genes associated with chitin polymer cleavage, the largest proportions were assigned to *Plesiomonas* and *Aeromonas*, at 25.93% and 17.33%, respectively, followed by *Bacteroides* (9.87%), *Millionella* (9.49%), and *Clostridium* (7.87%). For genes associated with chitooligosaccharide processing and chitobiose utilization, the leading candidate source genera were *Candidatus* Avirikenella (22.17%) and *Ruthenibacterium* (12.27%), whereas *Clostridium* and *Candidatus Microsyncoccus* accounted for 7.50% and 7.48% of the assigned gene abundance, respectively. For genes associated with GlcNAc transport, *Cetobacterium* had the largest assigned proportion (37.42%), followed by *Thomasclavelia* (11.04%), *Clostridium* (8.25%), and *Longibaculum* (7.04%). For genes associated with intracellular metabolism, the largest proportions were attributed to *Mucinivorans* (13.78%), *Parabacteroides* (11.69%), and *Alistipes* (11.37%), with *Cetobacterium* accounting for 8.91%. Thus, the leading candidate source genera differed among functional stages, although their taxonomic profiles overlapped. In particular, *Clostridium* and *Cetobacterium* were linked to target genes involved in multiple stages.

Discussion

Decapods contributed more than 80% of stomach-content volume in both sexes,

confirming that crustaceans constitute a major component of the natural diet of *F. cancrivora*. This result is consistent with the predominance of crustaceans, including crabs, in *F. cancrivora* collected from brackish-water swamps and ditches in Singapore [14], the dominance of crabs (Brachyura) in the diet of *F. moodiei* sampled on Middle Andaman Island, India [47] and records of crab consumption by *F. cancrivora* in Bogor, West Java, Indonesia [48]. Although the relative importance of the families Grapsidae and Ocypodidae differs between the sexes, decapods account for a high proportion of the total volume of food consumed by both sexes, suggesting that the chitinous exoskeleton is an important structural component of the food processed by the digestive system of *F. cancrivora*. Natural diet data provide an important ecological context for interpreting feeding-related morphological and functional traits in wild animals [49]. This dietary pattern provides the ecological context for evaluating the digestive traits associated with processing mechanically resistant, chitin-rich foods.

The pronounced longitudinal folds and multidirectional muscle layers of the stomach are consistent with roles in accommodation, mixing, and propulsion of ingesta, potentially compensating for the limited oral processing typical of anurans [17]. The mucosa of the small intestine is highly folded and bears well-developed villi, whereas the lumen of the large intestine is relatively wide and features semilunar folds in the mucosa and submucosa. These structural adaptations facilitate the accommodation of larger volumes of chyme and ensure sufficient contact with chitinase during digestion, thereby promoting the absorption of chitin hydrolysates. Chitinase activity was detected at similar levels across the stomach, small intestine, and large intestine, indicating that

363 chitin hydrolysis may occur throughout the digestive tract. Lipase exhibits high activity
364 in the intestine, which may be associated with the breakdown and digestion of lipids in
365 the hepatopancreas of crabs [50]. Previous histological, biochemical, and molecular
366 studies have documented chitinase expression in the gastric mucosa and pancreas of
367 frogs [7, 8, 51]. Oshima et al. found that pancreatic chitinase from *Bufo japonicus*
368 cleaved crab-shell chitin with a specific activity up to 4.5 times that of a commercial
369 bacterial chitinase, indicating that endogenous chitinases can act directly on native
370 crustacean chitin in at least some anurans [8]. Zhang et al. found significantly higher
371 chitinase activity in *F. cancrivora* than in *F. multistriata* in both gastric tissue at pH 3.0–
372 5.0 and intestinal tissue at pH 4.0–6.0 [18]. This comparative evidence is consistent
373 with the chitinase activity detected across multiple digestive tract regions in the present
374 study and supports a relatively strong endogenous capacity for chitin hydrolysis in *F.*
375 *cancrivora*.

376 The chitin-related functional markers extended from polymer cleavage to
377 chitooligosaccharide processing, uptake of degradation products, and intracellular
378 utilization of N-acetylglucosamine (GlcNAc). Cross-referencing the CAZy and KEGG
379 annotations increased the specificity with which chitin-related target genes were
380 identified [28, 29]. Among these markers, GH18/GH19 genes associated with chitin
381 hydrolysis provided relatively clear upstream evidence for polymer cleavage [52-54],
382 whereas *nagZ* and *chbP* are involved in the further processing of chitooligosaccharides
383 or chitobiose [52, 53, 55, 56]. The phosphotransferase system (PTS) component
384 encoded by *nagE* is associated with GlcNAc uptake and phosphorylation [52, 54],

whereas *ngcE–ngcF–ngcG* is involved in the ABC-type uptake of chitin degradation products [57]. Once inside the cell, GlcNAc can be converted to fructose-6-phosphate (Fru-6-P) through reactions involving *nagK–nagA–nagB*, thereby linking it to central carbon metabolism [52, 54, 58]. These hydrolytic, uptake, and intracellular metabolic steps are supported by culture-based, mutational, or multi-omics evidence from *Vibrio*, *Aeromonas*, and other chitin-utilizing bacteria [52-54, 57]. Among the candidate bacterial genera, *Aeromonas* is known for its chitinolytic capacity and ability to utilize chitin-derived substrates [59]. *Plesiomonas* is commonly found in the intestinal microbiota of aquatic vertebrates, particularly freshwater fishes [60]. *Ruthenibacterium* is an anaerobic gut bacterium associated with carbohydrate fermentation [61], while *Cetobacterium* is involved in carbohydrate utilization and the production of short-chain fatty acids and vitamin B12 [62]. In contrast, the metabolic functions of *Candidatus* Avirikenella remain poorly characterized. Thus, the metagenomic analysis indicates that the gut microbial gene repertoire of *F. cancrivora* contains genes spanning a series of functional steps involved in the further processing and utilization of chitin degradation products [52-54, 57].

The respective roles of the host and gut microbiota should not be divided simply into two fixed, sequential stages. Studies integrating host digestive physiology with gut microbial analyses have similarly shown that the presence or composition of gut microbiota alone does not necessarily establish their contribution to a specific host physiological function [63]. Chitinase activity in host tissues provides direct phenotypic evidence of hydrolysis [7, 8, 51], whereas the microbial metagenome reflects the

genetic potential of the community to utilize chitin degradation products [12]. *F. cancrivora* had higher host chitinase activity than *F. multistriata* but a significantly lower abundance of gut microbial genes encoding GH18-family chitinases [18]. This finding does not conflict with the present study; Zhang et al. tested whether the relevant genes were enriched in *F. cancrivora* relative to *F. multistriata*, whereas the present study examined whether the gut microbial gene repertoire of *F. cancrivora* spanned the processing, uptake, and intracellular utilization of chitin cleavage products [18]. Taken together, the available evidence supports endogenous host chitinases as a relatively well-defined basis for chitin hydrolysis [7, 8, 18, 51], whereas the gut microbiota may further utilize the oligosaccharides and amino sugars generated by chitin hydrolysis [52, 54, 55, 64]. In other animals that consume chitin-rich foods, the retention of functional *CHIA* genes and acidic chitinase activity have also been associated with the utilization of invertebrate prey [4, 5, 65]. Studies of myrmecophagous mammals and predatory heteropterans have further shown that their gut microbial gene repertoires have the potential to utilize chitin and its degradation products [6, 10, 66]. It should be noted that tissue homogenates used for enzyme assays may include enzymes from surface-associated microbes, although the histological and molecular evidence supports a host origin for at least part of the chitinase activity. These studies support the separate evaluation of host hydrolytic phenotypes and microbial functional potential, but the present results do not yet demonstrate that the gut microbiota mediate the adaptation of *F. cancrivora* to a crab-based diet, nor do they directly establish metabolic synergy between the host and its gut microbiota [12, 67].

Stomach contents reflect food intake during the sampling period, whereas the gut microbiota of wild animals may also be influenced by season, location, and interindividual variation [67]. Metagenomic annotations reflect the available gene repertoire; whether the relevant genes are expressed and what they contribute metabolically still require functional validation [12]. Future studies could pair analyses of dietary composition, digestive enzyme activity, and microbial function within the same individuals to test the correspondence among these three lines of evidence [12, 67]. Controlled-feeding experiments combined with metatranscriptomics and metabolomics could assess how the relevant genes and metabolites respond to dietary crustacean input [12, 18]. Long-read sequencing or high-quality metagenome-assembled genomes (MAGs) could also be used to confirm the genomic assignment of genes involved in cleavage, uptake, and intracellular metabolism [12].

Conclusions

Decapods, particularly Grapsidae, Ocypodidae, and Palaemonidae, constituted a major component of the natural diet of *F. cancrivora* in both sexes, indicating that its digestive system routinely encounters mechanically resistant, chitin-rich animal foods. The gastrointestinal structural features and chitinase activity detected across the stomach, small intestine, and large intestine indicate an endogenous capacity for physical processing and hydrolysis of such foods. Gut metagenomes further contained genes associated with chitin polymer cleavage, chitooligosaccharide processing, transport of degradation products, and intracellular GlcNAc metabolism, with candidate source genera differing among functional stages. Together, these findings

show that the crustacean-rich diet of *F. cancrivora* corresponds to both host digestive traits and gut microbial functional potential, providing an integrated ecophysiological perspective on the utilization of chitin-rich animal foods.

Declarations

Ethics approval and consent to participate

All procedures involving animals were approved by the Animal Ethics Committee of the Hainan Ecological and Environmental Education Center (approval no. HNECEE-2020-003).

Consent for publication

Not applicable.

Availability of data and materials

The raw metagenomic sequencing data generated during this study have been deposited in the NCBI Sequence Read Archive (SRA) under BioProject accession PRJNA1524366. All other data generated or analysed during this study are included in this article and its additional file.

Competing interests

The authors declare that they have no competing interests.

Funding

This work was supported by the National Natural Science Foundation of China (grant number 32471587).

Authors' contributions

T.L.: Validation, formal analysis, investigation, data curation, writing – original draft,

visualization. M.C.: Investigation. M.H.: Conceptualization, writing – review and editing, supervision, project administration, funding acquisition. L.W.: Conceptualization, methodology, formal analysis, investigation, data curation. All authors read and approved the final manuscript.

Acknowledgements

We sincerely thank all laboratory members for their invaluable assistance with field sampling.

Additional files

File name: Additional file 1

File format: .docx

Title of data: Supplementary Tables S1–S4

Description of data: Supplementary data on dietary indices, prey-order IRI values, bacterial genera with reported chitin-degrading members, and candidate functional genes related to chitin utilization.

Figure Legends

Fig. 1. Composition of stomach contents recovered by flushing from male and female *F. cancrivora*. a. Relationship between the numerical percentage (N%) and volumetric percentage (V%) of prey at the order level. Point size represents the relative frequency of occurrence (F%), and gray lines connect values for the same prey order between the sexes. b. The 10 prey families with the highest index of relative importance (IRI) values. Circles and squares represent males and females, respectively, and horizontal lines connect values for the same prey family between the sexes. F% represents the number

of occurrences of each prey taxon as a percentage of the summed occurrences across all taxa. IRI values are displayed on a logarithmic scale.

Fig. 2. Histological architecture of the digestive tract in *F. cancrivora*. a. Dorsal surface of the tongue; b. ventral surface of the tongue; c-d. esophagus; e-f. gastric body; g. small intestine; h. large intestine.

CE, columnar epithelium; EG, esophageal gland; FiP, filiform papilla; FuP, fungiform papilla; GC, goblet cell; GG, gastric body gland; GP, gastric pit; LP, lamina propria; LG, lingual gland; ME, mucosal epithelium; ML, muscular layer; MM, muscularis mucosae; SU, submucosa; V, villus.

Fig. 3. Histological architecture of the liver and pancreas in *F. cancrivora*. a. Liver; b. pancreas. CAC, centroacinar cell; HS, hepatic sinusoid; ID, intercalated duct; PI, pancreatic islet; ILBD, interlobular bile duct; ILV, interlobular vein; PA, pancreatic acinus; PC, pigment cell.

Fig. 4. Gut microbial community composition and chitin-degrading genera in *F. cancrivora*. a. Genus-level composition of the gut microbiota. The 20 major taxa are shown individually, and all remaining taxa are grouped as Others. b. Mean relative abundances of 31 genera reported in the literature to include chitin-degrading members. Genera with mean relative abundances greater than 0.1% are shown individually, and the remaining 18 genera are grouped as Others. Mean relative abundances were calculated after normalization within each sample, with the six samples weighted equally.

Fig. 5. KEGG functional composition of the gut metagenomes of *F. cancrivora*. Major

KEGG Level 2 functional categories are shown for six gut metagenomic samples (LI_R1–LI_R6) based on KEGG annotations. Colors denote different functional categories, and the y-axis indicates their relative abundance within each sample.

Fig. 6. Potential microbial pathway for chitin utilization in *F. cancrivora*. The schematic on the left summarizes four functional stages: chitin polymer cleavage, chitooligosaccharide processing, GlcNAc transport, and intracellular metabolism. Blue text denotes the genes annotated at each stage, and the green dashed line indicates the GH94–ChbP-mediated route for chitobiose utilization. Pie charts on the right show the relative contributions of the major candidate genera within each functional stage; the remaining genera are grouped as Others.

References

1. Karasov WH, Martínez del Rio C, Caviedes-Vidal E. Ecological physiology of diet and digestive systems. Annu Rev Physiol. 2011;73:69-93.
2. Chen P, Lin A, McKittrick J, Meyers M. Structure and mechanical properties of crab exoskeletons. Acta Biomater. 2008;4:587-596.
3. Poshina DN, Raik SV, Poshin AN, Skorik YA. Accessibility of chitin and chitosan in enzymatic hydrolysis: a review. Polym Degrad Stab. 2018;156:269-278.
4. Emerling CA, Delsuc F, Nachman MW. Chitinase genes (CHIAs) provide genomic footprints of a post-Cretaceous dietary radiation in placental mammals. Sci Adv. 2018;4:eaar6478.
5. Kim D, Wang Y, Jung H, Field RL, Zhang X, Liu T, et al. A type 2 immune

circuit in the stomach controls mammalian adaptation to dietary chitin. Science. 2023;381:1092-1098.

6. Cheng S-C, Liu C-B, Yao X-Q, Hu J-Y, Yin T-T, Lim BK, et al. Hologenomic insights into mammalian adaptations to myrmecophagy. Natl Sci Rev. 2023;10:nwac174.

7. Fujimoto W, Suzuki M, Kimura K, Iwanaga T. Cellular expression of the gut chitinase in the stomach of frogs *Xenopus laevis* and *Rana catesbeiana*. Biomed Res. 2002;23:91-99.

8. Oshima H, Miyazaki R, Ohe Y, Hayashi H, Kawamura K, Kikuyama S. Isolation and sequence of a novel amphibian pancreatic chitinase. Comp Biochem Physiol B Biochem Mol Biol. 2002;132:381-388.

9. Zhang S, Teraoka H, Kaiya H, Kitazawa T. Motilin- and ghrelin-induced contractions in isolated gastrointestinal strips from three species of frogs. Gen Comp Endocrinol. 2021;300:113649.

10. Teullet S, Tilak M, Magdeleine A, Schaub R, Weyer N, Panaino W, et al. Metagenomics uncovers dietary adaptations for chitin digestion in the gut microbiota of convergent myrmecophagous mammals. mSystems. 2023;8:e00388-23.

11. Leonard A, Earth Hologenome Initiative Consortium, Alberdi A. A global initiative for ecological and evolutionary hologenomics. Trends Ecol Evol. 2024;39:616-620.

12. Worsley SF, Videvall E, Harrison XA, Björk JR, Mazel F, Wanelik KM. Probing

the functional significance of wild animal microbiomes using omics data. Funct Ecol. 2024;38:2329-2349.

13. Moran NA, Ochman H, Hammer TJ. Evolutionary and ecological consequences of gut microbial communities. Annu Rev Ecol Evol Syst. 2019;50:451-475.

14. Elliott AB, Karunakaran L. Diet of *Rana cancrivora* in fresh water and brackish water environments. J Zool. 1974;174:203-215.

15. Motani R, Vermeij GJ. Ecophysiological steps of marine adaptation in extant and extinct non-avian tetrapods. Biol Rev Camb Philos Soc. 2021;96:1769-1798.

16. Zheng Y, Zhang S, Lu Q, Zhang S, Wang L, Hong M, et al. Population genetic patterns of a mangrove-associated frog reveal its colonization history and habitat connectivity. Divers Distrib. 2021;27:1584-1600.

17. Schwarz D, Mielke M, Handschuh S, Herrel A, Lemell P, Cunha LD, et al. Beyond mammals: the evolution of chewing and other forms of oropharyngeal food processing in vertebrates. Biol Rev Camb Philos Soc. 2026;101:1406-1462.

18. Zhang Y, Chang Z-H, Gan S, Wang S-H, Luo J-X, Jin L, et al. Hologenomic rewiring facilitates dietary adaptation to chitin-rich marine resources in the crab-eating frog. Front Zool. 2026.

19. Richarson MRA, Ingram T. Effects of competition and predation risk from a life history intraguild predator on individual specialisation. J Anim Ecol. 2025;94:1811-1822.

20. Dollion A, Measey G, Cornette R, Carne L, Tolley K, da Silva J, et al. Does diet

583 drive the evolution of head shape and bite force in chameleons of the genus
584 *Bradypodion*? Funct Ecol. 2017;31:671-684.
585 21. Huang S, Lin J, Chou C, Liao C, Hsu J, Tsai J, et al. Dances with wolves: The
586 demographic consequence of asymmetric competition and intraguild predation
587 in a native-invasive skink system. Funct Ecol. 2023;37:614-624.
588 22. Chen S, Zhou Y, Chen Y, Gu J. fastp: an ultra-fast all-in-one FASTQ
589 preprocessor. Bioinformatics. 2018;34:884-890.
590 23. Langmead B, Salzberg SL. Fast gapped-read alignment with Bowtie 2. Nat
591 Methods. 2012;9:357-359.
592 24. Li D, Liu C-M, Luo R, Sadakane K, Lam T-W. MEGAHIT: an ultra-fast single-
593 node solution for large and complex metagenomics assembly via succinct de
594 Bruijn graph. Bioinformatics. 2015;31:1674-1676.
595 25. Hyatt D, Chen GL, Locascio PF, Land ML, Larimer FW, Hauser LJ. Prodigal:
596 prokaryotic gene recognition and translation initiation site identification. BMC
597 Bioinformatics. 2010;11:119.
598 26. Fu L, Niu B, Zhu Z, Wu S, Li W. CD-HIT: accelerated for clustering the next-
599 generation sequencing data. Bioinformatics. 2012;28:3150-3152.
600 27. Patro R, Duggal G, Love MI, Irizarry RA, Kingsford C. Salmon provides fast
601 and bias-aware quantification of transcript expression. Nat Methods.
602 2017;14:417-419.
603 28. Kanehisa M, Furumichi M, Sato Y, Kawashima M, Ishiguro-Watanabe M.
604 KEGG for taxonomy-based analysis of pathways and genomes. Nucleic Acids

Res. 2023;51:D587-D592.

29. Cantarel BL, Coutinho PM, Rancurel C, Bernard T, Lombard V, Henrissat B. The Carbohydrate-Active enZymes database (CAZy): an expert resource for glycogenomics. Nucleic Acids Res. 2009;37:D233-D238.

30. Buchfink B, Reuter K, Drost H. Sensitive protein alignments at tree-of-life scale using DIAMOND. Nat Methods. 2021;18:366-368.

31. Eddy SR. Accelerated profile HMM searches. PLoS Comput Biol. 2011;7:e1002195.

32. Olsen MA, Blix AS, Utsi TH, Sørmo W, Mathiesen SD. Chitinolytic bacteria in the minke whale forestomach. Can J Microbiol. 2000;46:85-94.

33. Zhang Y, Zhou Z, Liu Y, Cao Y, He S, Huo F, et al. High-yield production of a chitinase from *Aeromonas veronii* B565 as a potential feed supplement for warm-water aquaculture. Appl Microbiol Biotechnol. 2014;98:1651-1662.

34. Ramaiah N, Hill R, Chun J, Ravel J, Matte M, Straube W, et al. Use of a *chiA* probe for detection of chitinase genes in bacteria from the Chesapeake Bay. FEMS Microbiol Ecol. 2000;34:63-71.

35. Kim TI, Ki KS, Lim DH, Vijayakumar M, Park SM, Choi SH, et al. Novel *Acinetobacter parvus* HANDI 309 microbial biomass for the production of N-acetyl-β-d-glucosamine (GlcNAc) using swollen chitin substrate in submerged fermentation. Biotechnol Biofuels. 2017;10:59.

36. Raimundo I, Silva R, Meunier L, Valente SM, Lago-Lestón A, Keller-Costa T, et al. Functional metagenomics reveals differential chitin degradation and

627 utilization features across free-living and host-associated marine microbiomes.
628 Microbiome. 2021;9:43.
629 37. Middelboe M, Traving S, Castillo D, Kalatzis P, Glud R. Prophage-encoded
630 chitinase gene supports growth of its bacterial host isolated from deep-sea
631 sediments. ISME J. 2025;19:wraf004.
632 38. Paulsen S, Andersen B, Gram L, Machado H. Biological potential of chitinolytic
633 marine bacteria. Mar Drugs. 2016;14:230.
634 39. Cai Y, Li X, Chen S, Liu Q, Lu H, Xie J, et al. Characterization and Optimization
635 of Fermentation Conditions of *Roseateles* sp. L2-2, a Novel Chitin-Degrading
636 Bacterium from the Intestine of *Odorrana margaretae*. Microorganisms.
637 2025;13:2033.
638 40. Chanworawit K, Wangsoonthorn P, Deevong P. Characterization of chitinolytic
639 bacteria newly isolated from the termite *Microcerotermes* sp. and their
640 biocontrol potential against plant pathogenic fungi. Biosci Biotechnol Biochem.
641 2023;87:1077-1091.
642 41. Khatun M, Khatun ML, Milon MA-A, Anzuman M, Alam MK, Jamal MAHM,
643 et al. Isolation, purification, and characterization of endochitinase producing
644 bacteria as potential bio-control agents of fungal phytopathogens. Nat Prod
645 Commun. 2025;20:1934578X251342013.
646 42. Leisner JJ, Vogensen FK, Kollmann J, Aideh B, Vandamme P, Vancanneyt M,
647 et al. α-chitinase activity among lactic acid bacteria. Syst Appl Microbiol.
648 2008;31:151-156.

649 43. Macdonald C, Barden S, Foley S. Isolation and characterization of chitin-
650 degrading micro-organisms from the faeces of Goeldi's monkey, *Callimico*
651 *goeldii*. J Appl Microbiol. 2014;116:52-9.
652 44. Sun X, Li J, Du J, Xiao H, Ni J. *Cellulomonas macrotermitis* sp. nov., a
653 chitinolytic and cellulolytic bacterium isolated from the hindgut of a fungus-
654 growing termite. Antonie Van Leeuwenhoek. 2018;111:471-478.
655 45. Winssy TD, Gopal NO, Indiragandhi P, Balasubramani V, Anandham R.
656 Chitinase producing gut-associated bacteria affected the survivability of the
657 insect *Spodoptera frugiperda*. Front Biosci 2024;16:15.
658 46. Xu J, Yang Y, Liu Y, Ran C, Li J, He S, et al. Characterization of an exo-chitinase
659 from a *Citrobacter* strain isolated from the intestine content of large yellow
660 croakers. Acta Microbiol Sin. 2016;56:1089-1104.
661 47. Vassilieva AB, Nguyen TD, Sorokin PA. Morphological diversity of tadpoles of
662 fork-tongued frogs (Anura: Dicroglossidae) with different trophic
663 specializations. Vertebr Zool. 2025;75:31-57.
664 48. Potapov A, Beaulieu F, Birkhofer K, Bluhm S, Degtyarev M, Devetter M, et al.
665 Feeding habits and multifunctional classification of soil-associated consumers
666 from protists to vertebrates. Biol Rev Camb Philos Soc. 2022;97:1057-1117.
667 49. Sugiura K, Takahira N, Wada T. Sexual dimorphism, allometric morphological
668 changes, and wild diet of the endemic Antarctic tardigrade Milnesium rastrum.
669 Zoological Lett. 2026;12:13.
670 50. Latyshev N, Kasyanov S, Kharlamenko V, Svetashev V. Lipids and of fatty acids

of edible crabs of the north-western Pacific. Food Chem. 2009;116:657-661.

51. Dandrifosse G. Purification of chitinases contained in pancreas or gastric mucosa of frog. Biochimie. 1975;57:829-31.

52. Getz LJ, Robinson OS, Thomas NA. Functional genomics of chitin degradation by *Vibrio parahaemolyticus* reveals finely integrated metabolic contributions to support environmental fitness. PLoS Genet. 2025;21:e1011370.

53. Larsbrink J, Zhu Y, Kharade SS, Kwiatkowski KJ, Eijsink VG, Koropatkin NM, et al. A polysaccharide utilization locus from *Flavobacterium johnsoniae* enables conversion of recalcitrant chitin. Biotechnol Biofuels. 2016;9:260.

54. Tugui CG, Sorokin DY, Hijnen W, Wunderer J, Bout K, van Loosdrecht MCM, et al. Exploring the metabolic potential of *Aeromonas* to utilise the carbohydrate polymer chitin. RSC Chem Biol. 2025;6:227-239.

55. McClure R, Rivas-Ubach A, Hixson K, Farris Y, Garcia M, Danczak R, et al. Multi-omics of a model bacterial consortium deciphers details of chitin decomposition in soil. mBio. 2025;16:e00404-25.

56. Park JK, Keyhani NO, Roseman S. Chitin catabolism in the marine bacterium *Vibrio furnissii*: Identification, molecular cloning, and characterization of A N, N'-diacetylchitobiose phosphorylase. J Biol Chem. 2000;275:33077-33083.

57. Xiao X, Wang F, Saito A, Majka J, Schlösser A, Schrempf H. The novel *Streptomyces olivaceoviridis* ABC transporter Ngc mediates uptake of N-acetylglucosamine and N,N'-diacetylchitobiose. Mol Genet Genomics. 2002;267:429-439.

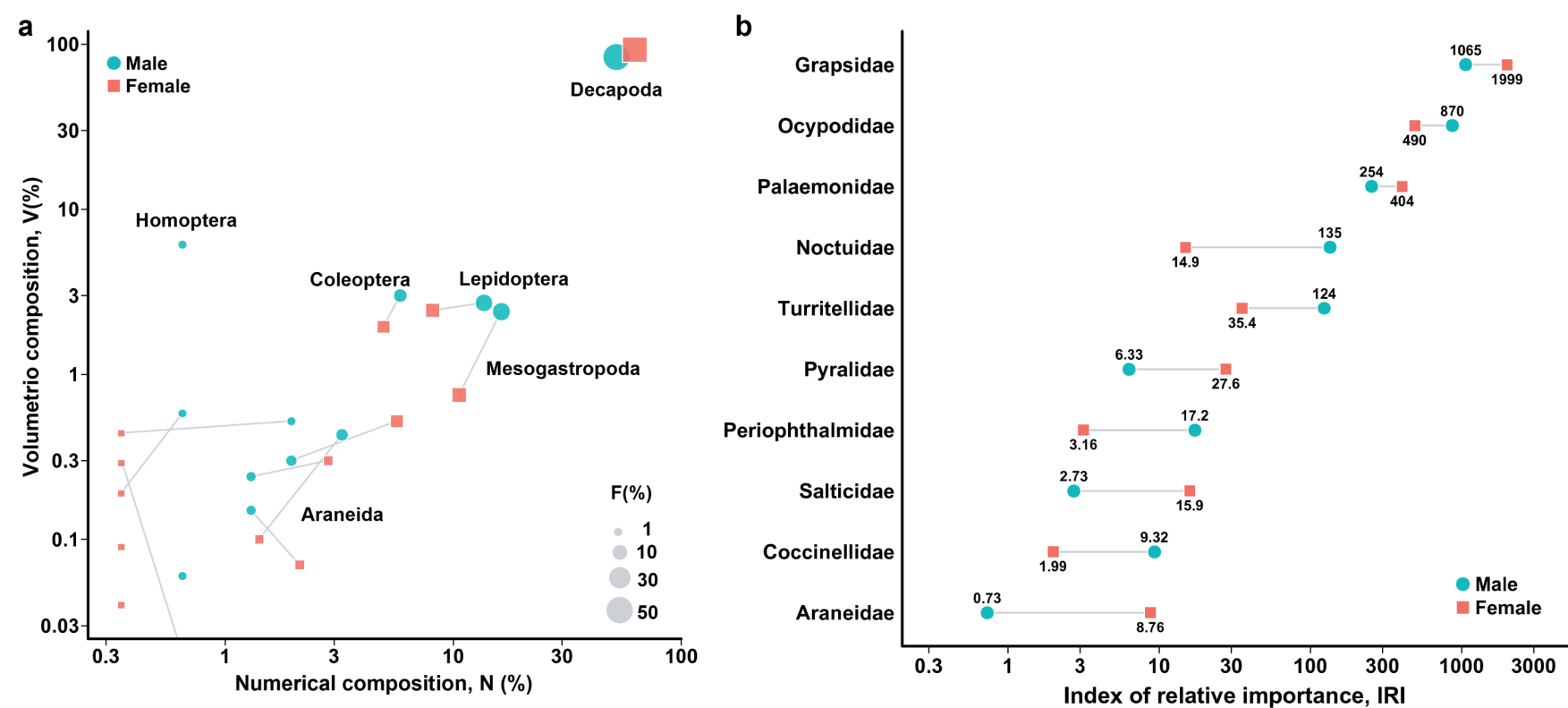
693 58. Park JT, Uehara T. How bacteria consume their own exoskeletons (turnover and
694 recycling of cell wall peptidoglycan). Microbiol Mol Biol Rev. 2008;72:211-
695 227.
696 59. Jangir Y, Guo Y, Connon S, Pontrelli S, Wu F, Schwartzman J, et al. Deep-sea
697 anaerobic microbial communities couple degradation of insoluble chitin to
698 extracellular electron transfer. ISME J. 2026;20:wrag151.
699 60. Stephens W, Burns A, Stagaman K, Wong S, Rawls J, Guillemin K, et al. The
700 composition of the zebrafish intestinal microbial community varies across
701 development. ISME J. 2016;10:644-654.
702 61. Hitch TCA, Masson JM, Pauvert C, Bosch J, Nüchtern S, Treichel NS, et al.
703 HiBC: a publicly available collection of bacterial strains isolated from the
704 human gut. Nat Commun. 2025;16:4203.
705 62. Qi X, Zhang Y, Zhang Y, Luo F, Song K, Wang G, et al. Vitamin B(12) produced
706 by Cetobacterium somerae improves host resistance against pathogen infection
707 through strengthening the interactions within gut microbiota. Microbiome.
708 2023;11:135.
709 63. Koito T, Ito Y, Suzuki A, Tame A, Ikuta T, Suzuki M, et al. Difference in sulfur
710 regulation mechanism between tube-dwelling and free-moving polychaetes
711 sympatrically inhabiting deep-sea hydrothermal chimneys. Zoological Lett.
712 2023;9:18.
713 64. Pontrelli S, Szabo R, Pollak S, Schwartzman J, Ledezma-Tejeida D, Cordero
714 OX, et al. Metabolic cross-feeding structures the assembly of polysaccharide

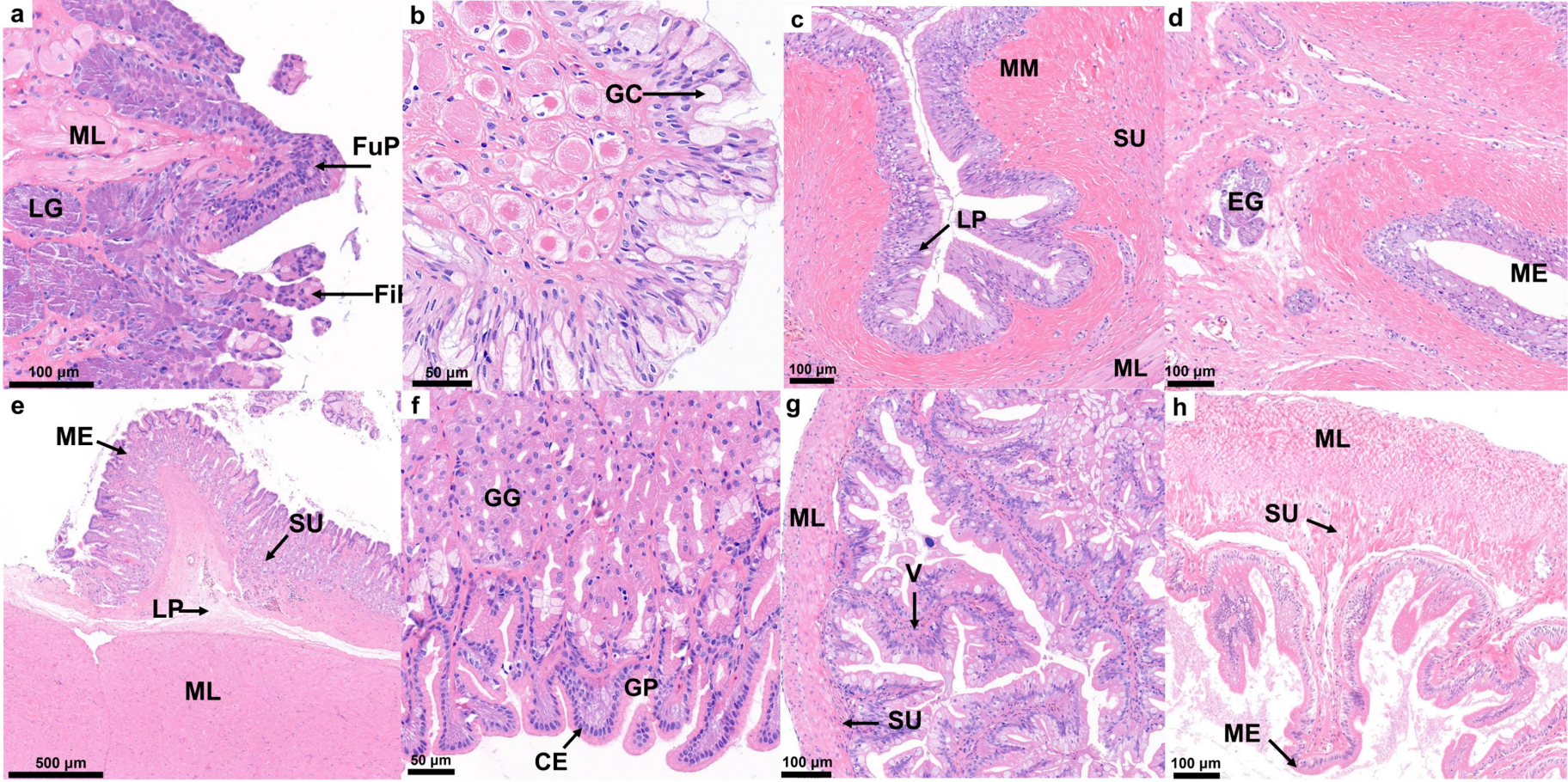
degrading communities. Sci Adv. 2022;8:eabk3076.

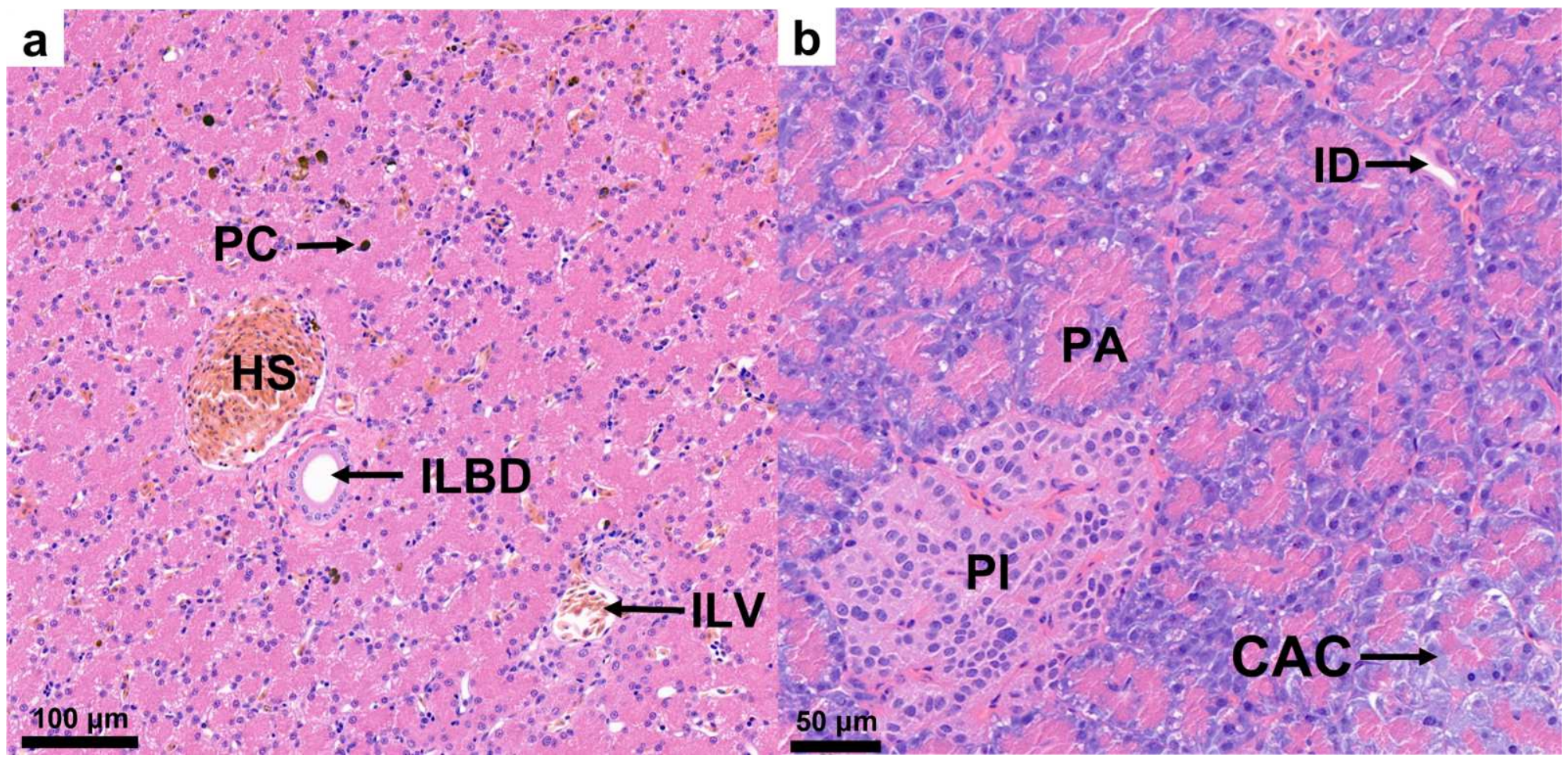
65. Tabata E, Itoigawa A, Koinuma T, Tayama H, Kashimura A, Sakaguchi M, et al. Noninsect-based diet leads to structural and functional changes of acidic chitinase in Carnivora. Mol Biol Evol. 2022;39:msab331.

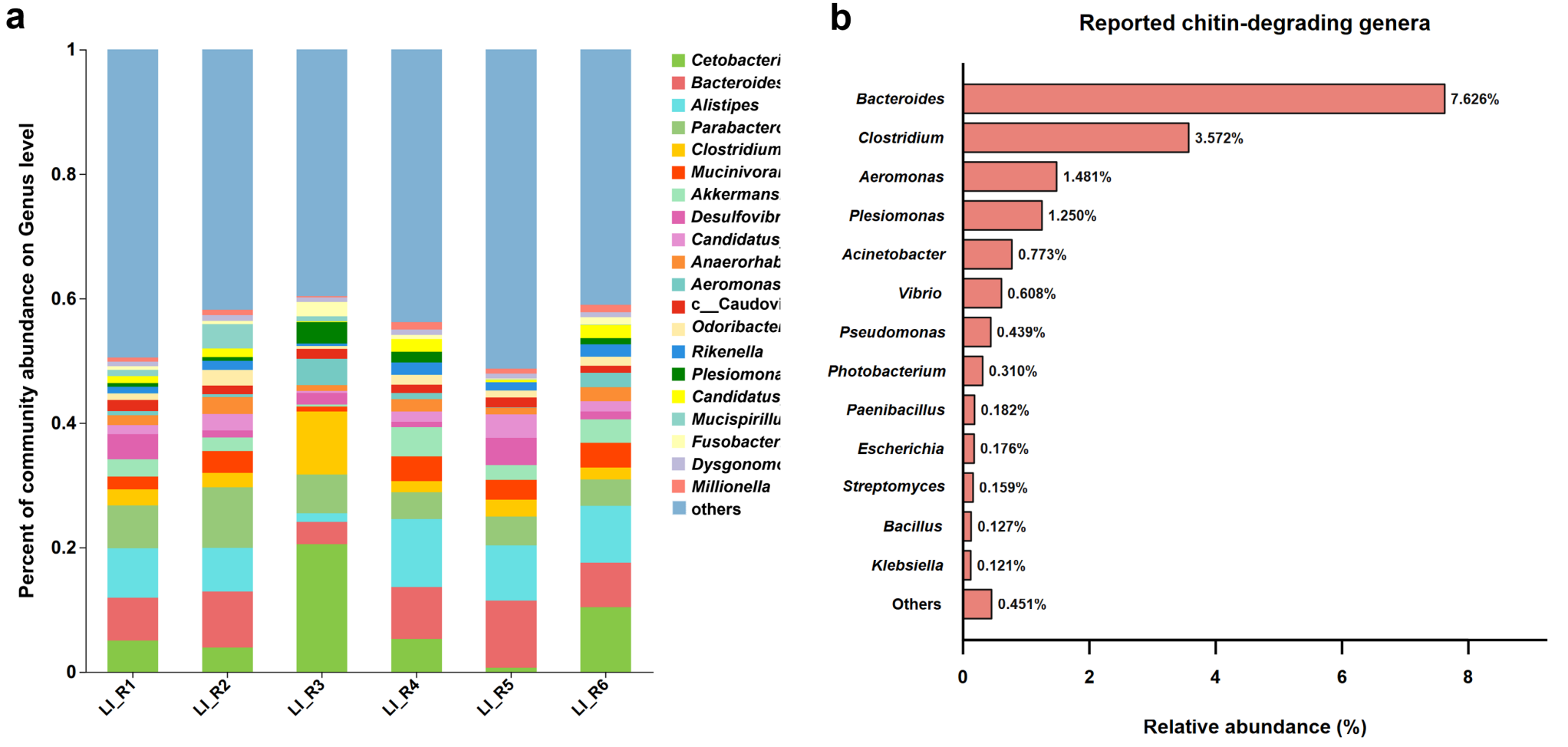
66. Sun J, Meng Y, Chen Z, Zhao T, Yang C, Chen S, et al. Gut microbiome convergence and functional adaptation underlie the evolution of predation in stink bugs (Heteroptera: Pentatomidae). Microbiome. 2026;14:56.

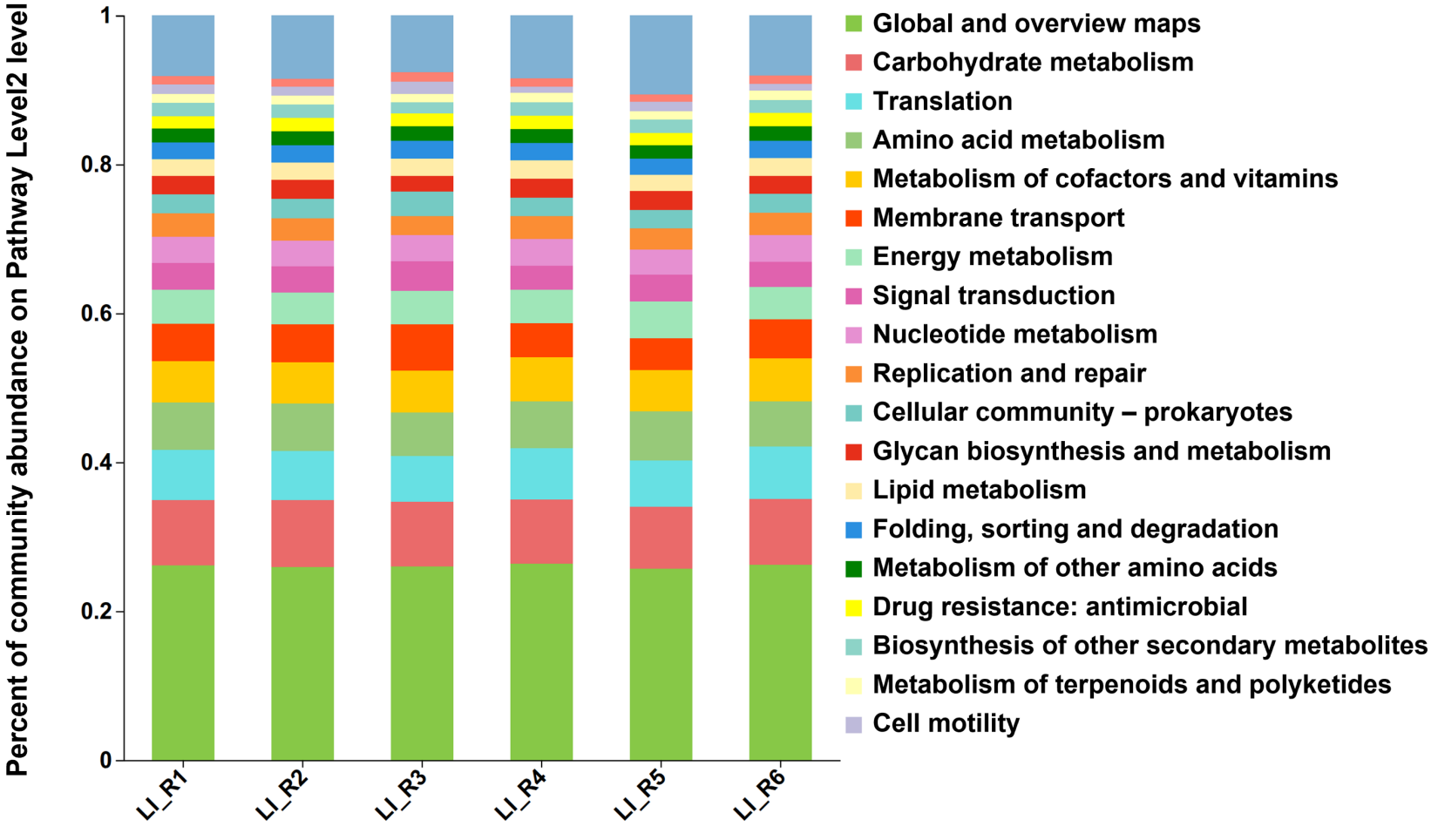
67. Fountain-Jones NM, Giraud T, Zinger L, Bik H, Creer S, Videvall E. Molecular ecology of microbiomes in the wild: common pitfalls, methodological advances and future directions. Mol Ecol. 2024;33:e17223.


a
Male
Female
Decapoda
Homoptera
Coleoptera
Lepidoptera
Mesogastropoda
Araneida
F(%)
1
10
30
50
Volumetrio composition, V(%)
Numerical composition, N (%)
100
30
10
3
1
0.3
0.1
0.03
0.3
1
3
10
30
100
b
Grapsidae
Ocypodidae
Palaemonidae
Noctuidae
Turritellidae
Pyralidae
Periophthalmidae
Salticidae
Coccinellidae
Araneidae
1065
1999
870
490
254
404
135
14.9
124
35.4
6.33
27.6
17.2
3.16
2.73
15.9
9.32
1.99
0.73
8.76
Male
Female
0.3
1
3
10
30
100
300
1000
3000
Index of relative importance, IRI

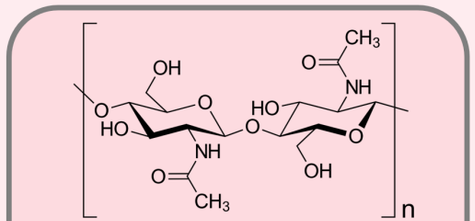

a
ML
FuP
LG
Fil
100 µm
b
GC
50 µm
c
MM
SU
LP
ML
100 µm
d
EG
ME
100 µm
e
ME
SU
LP
ML
500 µm
f
GG
GP
CE
50 µm
g
ML
V
SU
100 µm
h
ML
SU
ME
100 µm


a
PC
HS
ILBD
ILV
100 µm
b
ID
PA
PI
CAC
50 µm


a
Percent of community abundance on Genus level
1
0.8
0.6
0.4
0.2
0
LI_R1
LI_R2
LI_R3
LI_R4
LI_R5
LI_R6
Cetobacteri
Bacteroides
Alistipes
Parabacter
Clostridium
Mucinivora
Akkermans
Desulfovibr
Candidatus
Anaerorhab
Aeromonas
c__Caudovi
Odoribacte
Rikenella
Plesiomona
Candidatus
Mucispirillu
Fusobacter
Dysgonom
Millionella
others
b
Reported chitin-degrading genera
Bacteroides
Clostridium
Aeromonas
Plesiomonas
Acinetobacter
Vibrio
Pseudomonas
Photobacterium
Paenibacillus
Escherichia
Streptomyces
Bacillus
Klebsiella
Others
7.626%
3.572%
1.481%
1.250%
0.773%
0.608%
0.439%
0.310%
0.182%
0.176%
0.159%
0.127%
0.121%
0.451%
0
2
4
6
8
Relative abundance (%)


Percent of community abundance on Pathway Level2 level
1
0.8
0.6
0.4
0.2
0
LI_R1
LI_R2
LI_R3
LI_R4
LI_R5
LI_R6
Global and overview maps
Carbohydrate metabolism
Translation
Amino acid metabolism
Metabolism of cofactors and vitamins
Membrane transport
Energy metabolism
Signal transduction
Nucleotide metabolism
Replication and repair
Cellular community – prokaryotes
Glycan biosynthesis and metabolism
Lipid metabolism
Folding, sorting and degradation
Metabolism of other amino acids
Drug resistance: antimicrobial
Biosynthesis of other secondary metabolites
Metabolism of terpenoids and polyketides
Cell motility

Chitin polymer cleavage



GH18 chitinase, K01183
GH18 endo-chitodextrinase, K21606
GH19/GH19_1 putative chitinase, K03791

Chitooligosaccharides /Chitobiose

GH94–ChbP (K18675)
chitobiose phosphorolysis

GlcNAc+ GlcNAc-1-p

nagZ
GH3 x K01207

GlcNAc

Chitooligosaccharide processing

ngcE (K10200), ngcF (K10201), ngcG (K10202), ABC transporter

nagE (K02804), PTS

GlcNAc transport

GlcNAc

GlcNAc-6-P

nagK (K28207)

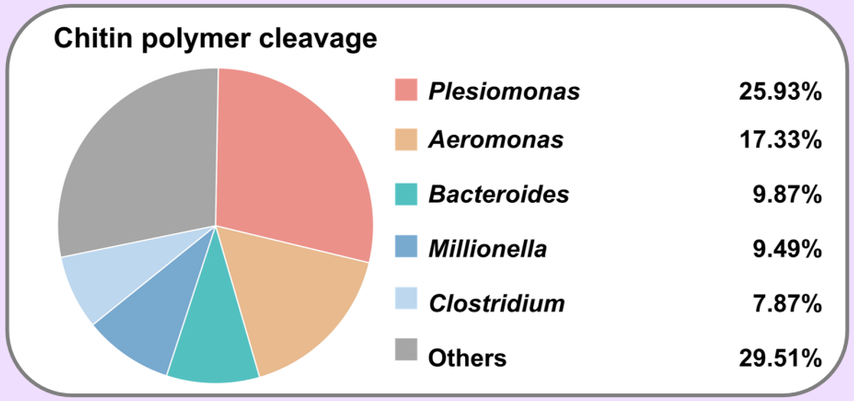
nagA(K01443)

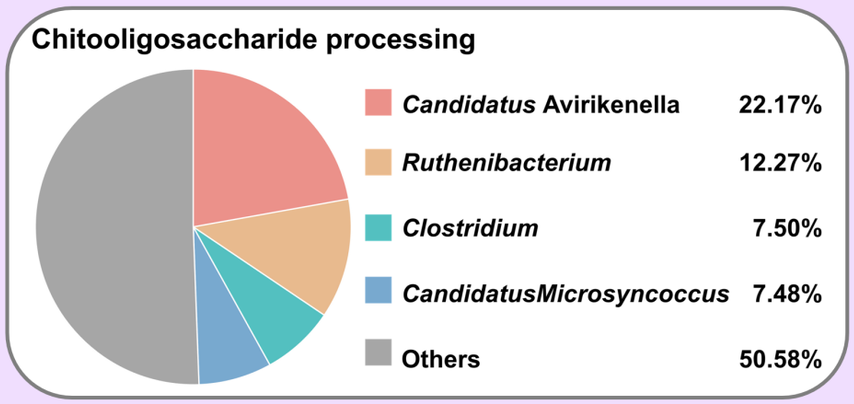
GlcN-6-P

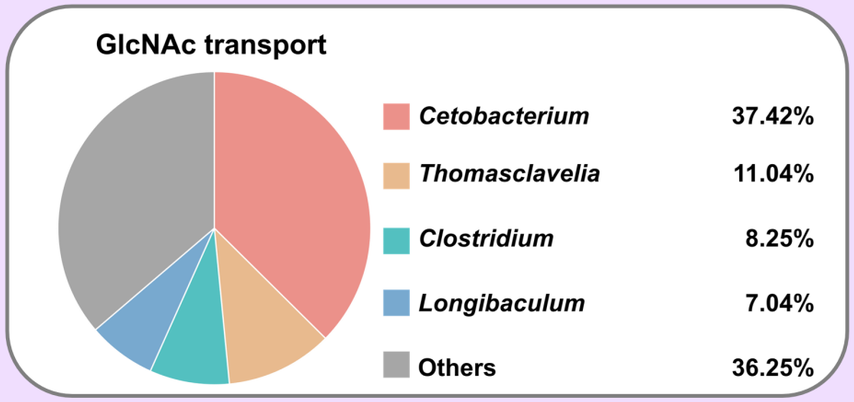
nagB(K02564)

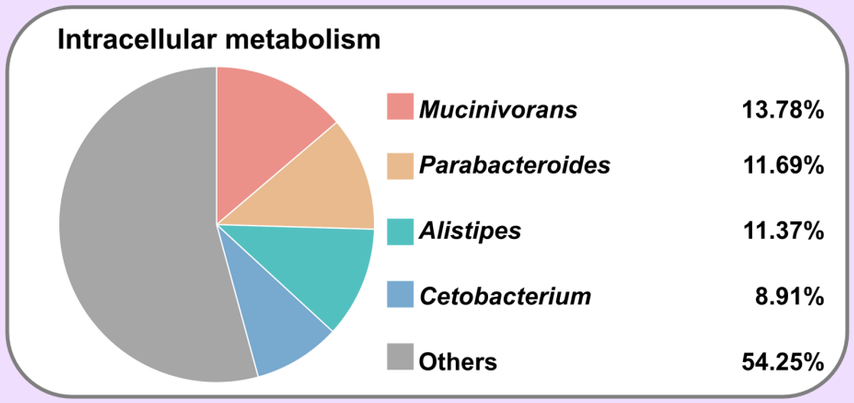
Fru-6-P

Intracellular metabolism









Supplementary Files

This is a list of supplementary files associated with this preprint. Click to download.

- Additionalfile.pdf